International Journal of Luminescence and applications
Vol6 (1) February, 2016, pages 25-34

Luminescence Studies of Dysprosium Doped Strontium Silicate Phosphor

Ishwar Prasad Sahu*, [a]D. P. Bisen, [b]Raunak Kumar Tamrakar

[a]School of Studies in Physics & Astrophysics, Pt. Ravishankar Shukla University, Raipur (C.G.)
Pin Code - 492010, India
[b]Department of Applied Physics, Bhilai Institute of Technology Durg (C.G.)
Pin Code - 491001, India
Corresponding author Email Id: **ishwarprasad1986@gmail.com***

Abstract
Dysprosium doped strontium silicate was prepared by solid state reaction method. X-ray diffraction (XRD) pattern of the sample confirmed that the synthesized phosphors had monoclinic structure. Energy dispersive X-ray spectroscopy (EDS) confirmed the presence of elements in the $Sr_2SiO_4:Dy^{3+}$ (2.0%) phosphor. Thermoluminescence (TL) parameters such as activation energy (E), order of kinetics (b), and the frequency factor (s) of phosphor were calculated using peak shape method. The prepared $Sr_2SiO_4:xDy^{3+}$ phosphors were excited at 351 nm and their corresponding emission spectra was recorded at blue (480 nm) and yellow (576 nm) line due to the $^4F_{9/2} \rightarrow {}^6H_{15/2}$, $^4F_{9/2} \rightarrow {}^6H_{13/2}$ transitions of Dy^{3+} ions. The possible mechanism of long lasting white light emitting $Sr_2SiO_4:Dy^{3+}$ (2.0%) phosphor was investigated. The mechanoluminescence (ML) intensity increased linearly with increasing impact velocity of the moving piston. The present investigation indicates that piezoelectricity was responsible to produce ML in the phosphor.

Keywords: XRD; Thermoluminescencc; Photoluminescence; CIE color coordinates; Mechanoluminescence.

Introduction

Long-lasting phosphorescence (LLP), a phenomenon due to the thermal stimulated recombination of holes and electrons at traps which leave holes or electrons in a long lived excited state at room temperature, is an interesting phenomenon in which the luminescence of LLP materials persists after the removal of the excitation source [1]. Since the LLP materials can be widely used in areas such as safety indication, emergency lighting, road signs, billboards, graphic arts, and interior decoration, many studies have been carried out on the synthesis technique[2].

In recent years, light emitting diode devices for general lighting purposes are of increasing interest. Hence, solid-state lighting (SSL) has become an interesting field for researchers especially with respect to white light sources. Particularly, white light-emitting-diodes (W-LEDs) receive lots of attention in the solid state lighting area for the replacement of conventional incandescent and fluorescent lamps, due to numerous advantageous properties such as high brightness, low power consumption, longevity, and good reliability, as well as excellent low-temperature performance [3, 4].

Dy^{3+} is one of the important rare earth ions which plays a major role in the production of different types of light-emitting materials. The luminescence spectrum of Dy^{3+} consists of two intense bands in the visible spectral range which correspond to the $^4F_{9/2} \rightarrow {}^6H_{15/2}$ (blue) and $^4F_{9/2} \rightarrow {}^6H_{13/2}$ (yellow) transitions [5]. At the moment, many researchers are engaged in studies on the luminescent properties of Dy^{3+} ions incorporated in various compounds.

ML has found various important applications such as impact sensors in spacecrafts (the emission intensity can be used to determine the kinetic energy of impact), fracture sensor, damage sensor, stress sensor etc. Thus, many researchers have been focused on the investigation of phosphors with high ML [6]. Until now, some phosphors with high ML, such as (red phosphor) $BaTiO_3$–$CaTiO_3$:Pr, (green phosphor) $SrAl_2O_4$:Eu, (yellow phosphor) ZnS:Mn, and (blue phosphor) $CaYAl_3O_7$:Eu etc., have been developed. However, the requirement of ML sensors is still incomplete with the development of new materials. More ML phosphors with strong ML intensity and high stability are needed [7, 8].

It is well known that silicates have a higher physical and chemical stability after water treatment. In this paper, we report the synthesis of $Sr_2SiO_4:xDy^{3+}$ phosphors with different concentration (x = 1.0, 1.5, 2.0, 2.5 and 3.0 mol%) phosphor by high temperature solid state reaction method; further the structural characterization using XRD, FESEM, EDX analysis was done. Thermoluminescence (TL), photoluminescence (PL), long afterglow and mechanoluminescence (ML) luminescence of the phosphor were also investigated

Experimental
Material Preparation

$Sr_2SiO_4:xDy^{3+}$ phosphors (x = 1.0, 1.5, 2.0, 2.5 and 3.0 mol%) were prepared by high temperature solid state reaction method. The raw materials are strontium carbonate [$SrCO_3$ (99.90%)], silicon di-oxide [SiO_2 (99.99%)] and dysprosium oxide [Dy_2O_3 (99.99%)], all of analytical grade (A.R.), were employed in this experiment. Small amount of

boric acid (H_3BO_3) was added as flux. Initially, the raw materials were weighed according to the nominal compositions of $Sr_2SiO_4:xDy^{3+}$ phosphors. Then the powders were mixed and milled thoroughly for 2 hour using mortar and pestle. The ground sample was placed in an alumina crucible and subsequently fired at 1200ºC for 3 hours. The products were finally ground into powder for characterizing the phosphors. Solid state reaction method is widely used to prepare silicate phosphors because samples prepared using this method has good luminescence and very good morphology [9].

Structural and Luminescence Characterization Technique

The crystal structure of the prepared $Sr_2SiO_4:xDy^{3+}$ phosphors were characterized by powder XRD analysis. Powder XRD pattern has been obtained from Bruker D8 advanced X-ray powder diffractometer and the data were collected over the 2θ range 10º-80º. The X-rays were produced using a sealed tube (CuKα) radiation source and the wavelength of X-ray was (1.54060 Å). The crystal structure of the prepared sample was verified with the help of Joint Committee of Powder Diffraction Standard Data (JCPDS) file. (JCPDS: 39-1256). The morphological images of prepared phosphor were collected by the FESEM. The sample was coated with a thin layer of gold (Au) and then the surface morphology of prepared phosphor was observed by FESEM; ZIESS Ulta Plus-55 operated at the acceleration voltage of 15 kV. Energy dispersive X-ray spectroscopy (EDS) was used for the elemental (qualitative and quantitative) analysis of the prepared phosphor. The TL glow curves were recorded with the help of TLD reader 1009I by Nucleonix (Hyderabad, India Pvt. Ltd.). The excitation and emission spectra were recorded on a Shimadzu (RF 5301-PC) spectrofluorophotometer using the Xenon lamp (365 nm) as excitation source when measuring. The color chromaticity coordinates were obtained according to Commission International de I'Eclairage (CIE) 1931. The ML measurement was observed by a home made lab system comprising of RCA-931A photomultiplier tube (PMT). The ML glow curve can be plotted with the help of SM-340 application software installed in a computer attached with the storage oscilloscope [10, 11]. All measurements were carried out at the room temperature.

Results and Discussions

XRD Analysis

The typical XRD patterns of $Sr_2SiO_4:xDy^{3+}$ phosphors with different concentration (x = 1.0, 1.5, 2.0, 2.5 and 3.0 mol%) with that of the standard JCPDS file are shown in Fig. 1.

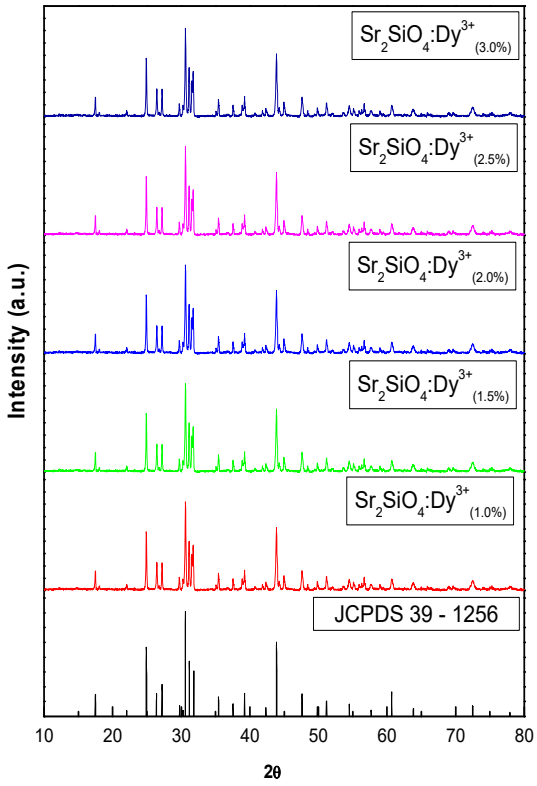

Fig. 1 XRD pattern of $Sr_2SiO_4:xDy^{3+}$ phosphors with standard JCPDS file

Nearly, all the diffraction peaks of the prepared phosphor matched well with Joint Committee Powder Diffraction Standard data (JCPDS) file (JCPDS: 39-1256) [12]. The crystal structure of the $Sr_2SiO_4:xDy^{3+}$ phosphors were monoclinic structure with space group C12/c1. The small amount of impurity did not change the crystal ctructure of the sintered phosphors. The radius of Dy^{3+} (0.99 Å) are very close to that of Sr^{2+} (about 1.12 Å) rather than Si^{4+} (0.41 Å). Therefore, the Dy^{3+} ions are expected to occupy Sr^{2+} sites in the host lattice.

Field Emission Scanning Electron Microscopy (FESEM)

The morphologies of prepared $Sr_2SiO_4:Dy^{3+}$ (2%) phosphor was observed by means of FESEM (Fig. 2). The surface of phosphor has shown irregular shapes. From the image, it can be observed that the prepared phosphor consists of particles with different size distribution. The morphological images showed that the particles were aggregated due to the high temperature synthesis.

International Journal of Luminescence and applications
Vol6 (1) February, 2016, pages 25-34

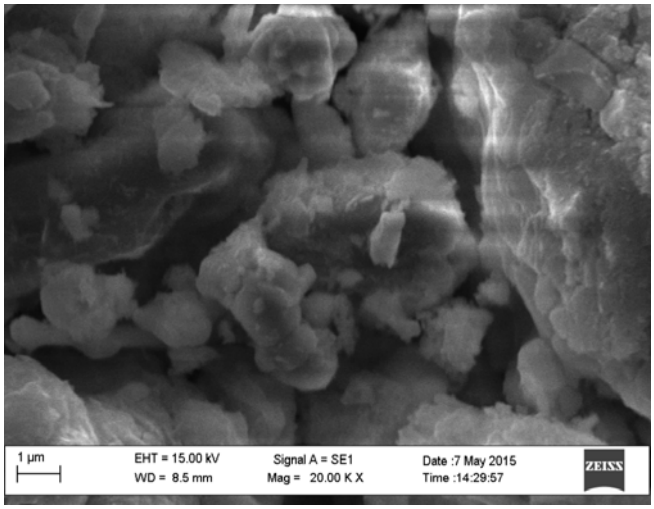

Fig. 2 FESEM imge of $Sr_2SiO_4:Dy^{3+}$ (2.0%) phosphor

Energy dispersive X-ray spectroscopy (EDS)

Fig. 3 shows the an Energy dispersive x-ray spectroscopy (EDS) spectra of $Sr_2SiO_4:Dy^{3+}$(2.0%) phosphor. (Sr), silicon (Si), oxygen (O) and dysprosium (Dy) were observed in EDS spectra of the sample, confirming the formation of $Sr_2SiO_4:Dy^{3+}$ (2.0%) phosphor.

Table 1 shows the compositional elements of $Sr_2SiO_4:Dy^{3+}$ (2.0%) phosphor, which is compared with the standard element. The elements appear in ratios concomitant with the proportions mixed in the starting materials

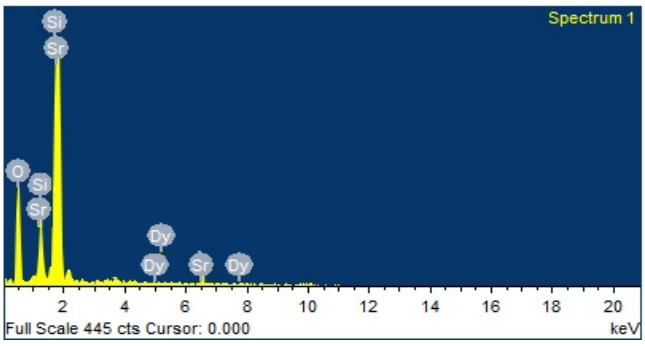

Fig. 3 EDS spectra of $Sr_2SiO_4:Dy^{3+}$ (2.0%) phosphor

Table 1 Compositio of elements in $Sr_2SiO_4:Dy^{3+}$ (2.0%) phosphor

Sr. N.	Standard	Elements	Weight %	Atomic %
1	SiO_2	O K	43.18	64.17
2	SiO_2	Si K	15.00	12.70
3	SrF_2	Sr L	27.02	16.03
4	DyF_3	Dy L	8.86	1.30
Total			**99.99**	**99.99**

Thermoluminescence (TL)

Thermoluminescence (TL) glow curves contain information regarding the release of charge from trapping sites at different temperatures, which is related to the trap depth. Additionally, measurement of the emission spectra can reveal differences between the types of recombination site and/or distinguish between electron and hole release. [13].

In order to study the trap states of the prepared $Sr_2SiO_4:Dy^{3+}$ (2.0%) phosphor, the TL glow curves were measured and are shown in Fig. 4. The phosphors were first irradiated for 10 min using 365 nm UV source, then the irradiated samples were heated at a linear heating rate of 5°C/s, from room temperatures to 300°C. Two TL glow peaks are located at 77.2 °C and 244.5 °C for $Sr_2SiO_4:Dy^{3+}$ (2.0%) phosphor corresponding to two different traps formed due to defects created in substituting Sr^{2+} by Dy^{3+} ions. The depths of the traps were calculated to be 0.75 eV for 77.2 °C. The dominant peak situated at 77.2 °C is responsible for the long-lasting phosphorescence in present case.

The first isolated peak situated at 77.2 °C was assigned as due to the formation of only one type of luminescence center, created by UV irradiation. It is also known that the doping with Dy^{3+} ions increases the lattice defects which existed already in the host. The calculated TL parameters are listed in Table 2.

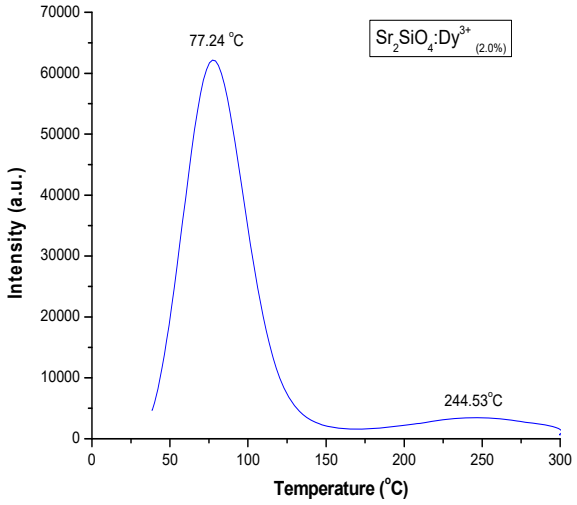

Fig. 4 TL glow curve of $Sr_2SiO_4:Dy^{3+}$ (2.0%) phosphor for 10 min UV irradiation

International Journal of Luminescence and applications
Vol6 (1) February, 2016, pages 25-34

Determination of kinetic parameters

There are various methods for evaluating the trapping parameters from TL glow curves [14]. For example, when one of the TL glow peaks is highly isolated from the others, the experimental method such as peak shape method is a suitable method to determine kinetic parameters. The TL parameters for the prominent glow peak of prepared phosphor was calculated using the peak shape method [15]. Fig. 5 shows the schematic diagram of glow curve peak shape method.

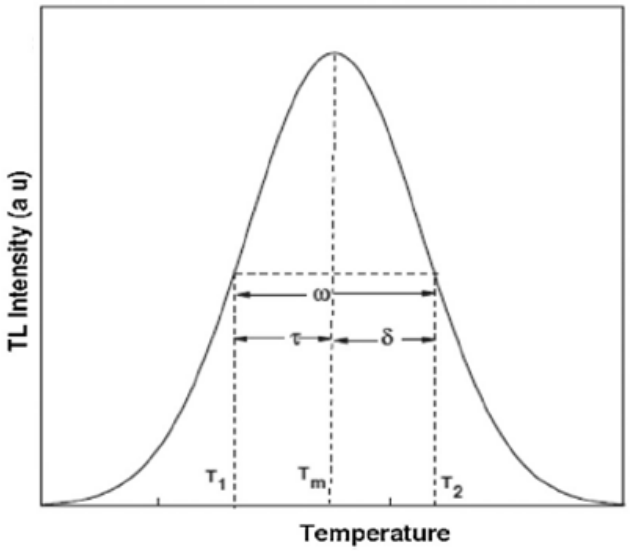

Fig. 5 Schematic diagram of glow curve peak shape method

Glow curve peak shape method: Using the glow curve peak shape method, the different shape parameters of the $Sr_2MgSi_2O_7:Eu^{3+}$ phosphor namely the total half intensity ω = T_2 - T_1 (τ+δ), τ is the half width at the low temperature side of the peak or the low temperature half width (τ = T_m-T_1); δ is the half width towards the fall-off side of the glow peak or the high temperature half width (δ = T_2-T_m), and T_m is the peak temperature and T_1 and T_2 are temperature on either side of T_m corresponding to half peak intensity, were determined [16].

Order of kinetics (*b*): The mechanism of recombination of de-trapped charge carriers with their counterparts is known as the order of kinetics (*b*). The order of kinetics can be predicted from shape of glow curve by using symmetry factor or geometric factor (μ_g) stated by Chen can be given as

$$\mu_g = \delta/\omega = T_2\text{-}T_m/T_2\text{-}T_1 \qquad (1)$$

The symmetry factor is to differentiate between first and second order TL glow peak. (μ_g) = 0.39-0.42 for the first order kinetics; (μ_g) = 0.49-0.52 for the second order kinetics and (μ_g) = 0.43-0.48 for the mixed order of kinetics [17].

Activation energy (E): The trap depth has been calculated by different methods proposed by several authors [18]. Trap depth for second order kinetics is calculated using the equation (2)

$$E = 2kT_m\left(1.76\frac{T_m}{\omega} - 1\right) \qquad (2)$$

Where, k is Boltzmann constant, E is activation energy, T_m is temperature of peak position.

Frequency factor (s): Frequency factor reflects the probability to escape of electrons from the traps after exposure of ionizing radiation and it is one of the important parameter of the phosphor characterization. Once the order of kinetics and activation energy were determined, the frequency factor (s) can be calculated from the equation (3)

$$\frac{\beta E}{kT_m^2} = s\left[1 + (b-1)\frac{2kT_m}{E}\right]\exp(E/KT_m) \qquad (3)$$

where b is order of kinetics, and β is the heating rate. In the present work β = 5°Cs^{-1}.

The calculated kinetic parameters of $Sr_2SiO_4:Dy^{3+}$(2.0%) phosphor by the peak shape method is given in Table 2. In our case, the value of shape factor (μ_g) is 0.53, which indicates that it is a case of second order kinetics, responsible for deep trap depth [19].

Table 2 Activation Energy (E), Frequency Factor (s^{-1}) and Shape factor (μ_g) for UV irradiated $Sr_2SiO_4:Dy^{3+}$ (2.0%) phosphor

UV Min	HTR	T_1 (°C)	T_m (°C)	T_2 (°C)
10	5	55.60	77.2	101.50

τ	δ	ω	μ = δ/ω	Activation Energy (eV)	Frequency Factor (sec^{-1})
21.64	24.26	45.90	0.53	0.75	2.96x 10^{10}

Photoluminescence (PL)

International Journal of Luminescence and applications
Vol6 (1) February, 2016, pages 25-34

The excitation and emission spectra of the phosphor were recorded and shown in Fig. 6 (a, b). The excitation spectrum of prepared $Sr_2SiO_4:Dy^{3+}$ (2.0%) phosphor under 576 nm emission is shown in Fig. 6 (a). In Fig. 6 (a), the excitation spectrum of $Sr_2SiO_4:Dy^{3+}$ (2.0%) phosphor, the peaks from 200–400 nm are due to 4f–4f transitions of Dy^{3+} ions. The excitation spectrum shows strong absorption at 351 nm and less intense absorptions at 327, 340, 368 and 38* nm due to transitions of Dy^{3+} [20, 21]. The peak of Dy^{3+} ion at 351 nm is near UV excitation. The emission spectrum of $Sr_2SiO_4:xDy^{3+}$ phosphor under excitation at 351 nm is shown in fig.6. It has two groups of emissions located at blue (480 nm) and yellow (576 nm) position were observed. Blue emission is less intense than the yellow emissions. These transitions have been identified as $^4F_{9/2} \rightarrow {}^6H_{15/2}$ and $^4F_{9/2} \rightarrow {}^6H_{13/2}$ transitions of Dy^{3+} respectively. It may be noted that the emission lines of Dy^{3+} are broadened somewhat, because there are several Stark levels for the $^4F_{9/2} \rightarrow {}^6H_J$ levels [22].

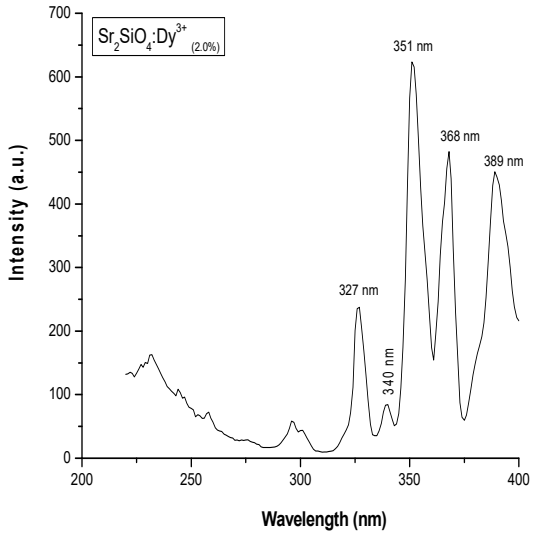

Fig. 6(a) Excitation spectra of $Sr_2SiO_4:xDy^{3+}$ (2.0%) phosphors

It is well known that the blue emission at 480 nm ($^4F_{9/2} \rightarrow {}^6H_{15/2}$) corresponds to the magnetic dipole transition, which hardly varies with the crystal field strength around Dy^{3+} ions, while the stronger yellow emission at 576 nm ($^4F_{9/2} \rightarrow {}^6H_{13/2}$) belongs to the hypersensitive forced electric dipole transition, which is strongly influenced by the outside surrounding environment. According to the Judd–Ofelt theory [23], when Dy^{3+} locates at a low symmetry local site (without inversion symmetry), yellow emission according to the electric dipole transition ($^4F_{9/2} \rightarrow {}^6H_{13/2}$) will be dominant. Conversely, a magnetic dipole transition ($^4F_{9/2} \rightarrow {}^6H_{15/2}$) will predominate in the emission spectra, resulting in a strong blue emission. In our case, the yellow emission ($^4F_{9/2} \rightarrow {}^6H_{13/2}$) dominates. The strong yellow emission is also beneficial to decrease the color temperature of the phosphor and generate warm white light emission [24]. It is well known that the ($^4F_{9/2} \rightarrow {}^6H_{13/2}$) transition is hypersensitive and therefore, its intensity strongly depends on the host, while the ($^4F_{9/2} \rightarrow {}^6H_{15/2}$) transition is less sensitive to the host. The optical properties of the material are often influenced by the structure of the matrix and synthesis technique [25].

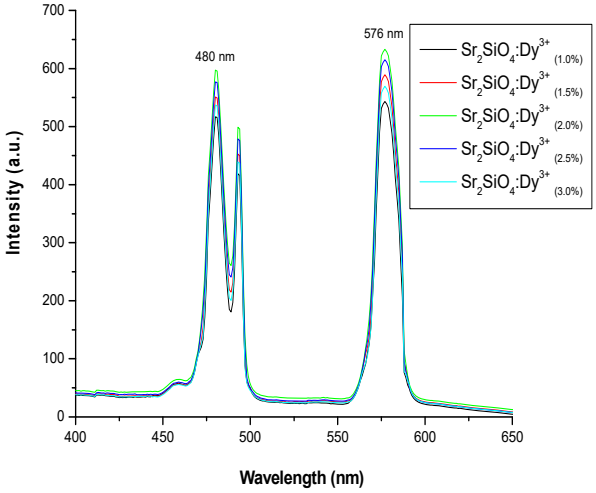

Fig. 6 Excitation and emission spectra of $Sr_2SiO_4:xDy^{3+}$ phosphors

When trivalent metallic ions, such as Dy^{3+} are incorporated into a host lattice and substitute divalent metallic ions, the charge balancing is required. Due to these chemically nonequivalent substitutions, an excess of positive charge in the host lattice must be compensated. One possible way of charge compensation mechanism is that two Dy^{3+} ions replace three Sr^{2+} ions to balance the charge of these phosphors, which create two $Dy^{\bullet}_{Sr}$ positive defects and one V''_{Sr} negative defect.

$$2\,DyDy + 3\,SrSr \rightarrow 2\,Dy^{\bullet}_{Sr} + V''_{Sr}$$

For $Sr_2SiO_4:xDy^{3+}$ the incorporation of alkali metal ions can neutralize the charge generated by Dy^{3+} substitution for Sr^{2+}, and thus stabilize the structure and enhance the luminescence. Dy^{3+} ions have been often used as co-dopants in the previously developed aluminate and silicate based materials. When divalent alkaline earth ions, such as Sr^{2+}, Ca^{2+}, Ba^{2+}, is substituted by trivalent Dy^{3+} in the alkaline earth silicates and aluminates, various defects can be induced due to the charge compensation mechanism among which alkaline earth ion vacancy, V_M, is the principal one. V_M is supposed to be the hole trap, while Dy^{3+} occupying alkaline earth ion sites is a very probable

source of electron trap. In the Eu^{2+} and the Dy^{3+} co-doped long afterglow materials, most of the excitation energy will be transferred from the host or the Dy^{3+} to the Eu^{2+}; thus only 5d-4f emissions of Eu^{2+} can be observed [26].

However, in Dy^{3+} singly doped sample, Dy^{3+} is not only the supplier of traps but also an activator itself. On the basis of the TL curve and the photoluminescence spectra results, it is reasonable to postulate that, (a) when Dy^{3+} doped into Sr_2SiO_4:xDy^{3+} host, due to the chemically nonequivalent substitution, Dy^{3+} ions create the electron traps during the high temperature synthesis process; (b) the long-lasting phosphorescence originates due to energy transfer from the electron traps to the Dy^{3+} ions, which give rise to the characteristic emissions of Dy^{3+}. A process of emitting the white light in Sr_2SiO_4:xDy^{3+} phosphor is illustrated schematically in Fig. 7.

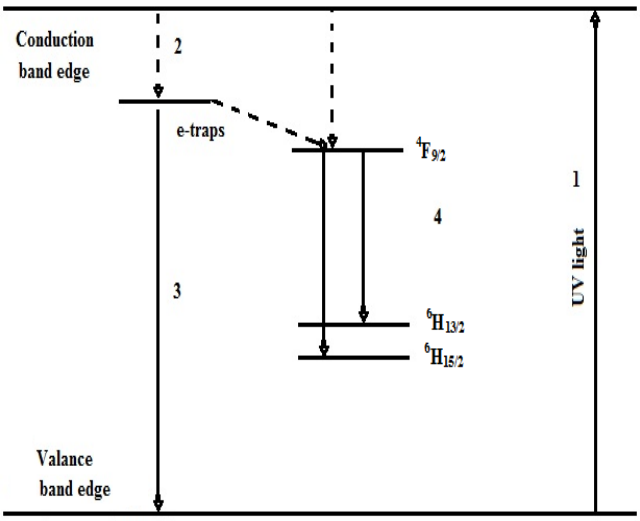

Fig. 7 The possible process of the origin of the long lasting phosphorescence in the Sr_2SiO_4:xDy^{3+} phosphor

After irradiation by UV light, the electrons in the valence band are excited to the conduction band and free electrons and holes are formed in the sample host. The holes or electrons were trapped by defect centers, released by heat at room temperature, and recombined with electrons or holes trapped by other defect centers (step1). One part of the excited electrons returned to the electron traps by the non-radiative way, and got stored in the electron traps, which were created at high temperature during the synthesis process (step 2). Because the electron traps are in a metastable state at room temperature, the excited electrons stored in it can be thermally released and be turned back to the valence band edge (step 3). After turning off the excited source, a majority of excited electrons stored in the electron traps would be transferred to the $^4F_{9/2}$ state of Dy^{3+} ions and would create the characteristic emissions of Dy^{3+} ions (step 4). When the decay ratio of the energy transfer from the electron traps to the $^4F_{9/2}$ state of Dy^{3+} ions is proper, the white light-emitting long-lasting phosphorescence of Dy^{3+} can be obtained. In the practical system, the electron traps and the hole traps may not be equally abundant or important in terms of their contribution to the white light emission, as suggested in Fig. 7 [27, 28].

CIE Chromaticity Coordinate

The luminescence color of the samples excited under 351 nm has been characterized by the CIE (Commission International de I'Eclairage) 1931 chromaticity diagram [29]. The emission spectrum of the Sr_2SiO_4:$Dy^{3+}_{(2.0\%)}$ phosphor was converted to the CIE 1931 chromaticity using the photoluminescent data and the interactive CIE software (CIE coordinate calculator) diagram as shown in Fig. 8.

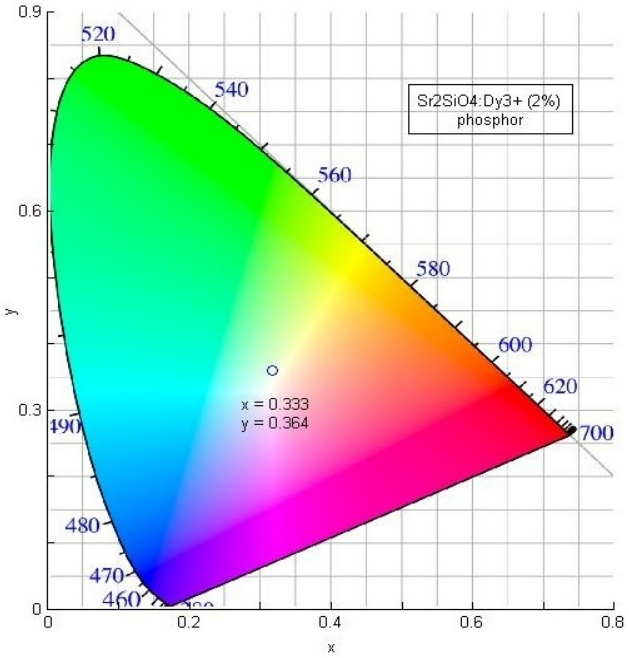

Fig. 8 CIE chromaticity diagram of Sr_2SiO_4:$Dy^{3+}_{(2.0\%)}$ phosphor

Luminescence colors of Sr_2SiO_4:$Dy^{3+}_{(2.0\%)}$ phosphor are placed in the near white light (x = 0.333, y = 0.364), corners.

Long Afterglow

Fig. 9 shows the typical afterglow curves of Sr_2SiO_4:$Dy^{3+}_{(2.0\%)}$ phosphor. The initial afterglow intensity of the sintered Sr_2SiO_4:$Dy^{3+}_{(2.0\%)}$ phosphor was high. The decay times of phosphor can be calculated by a curve fitting technique, and decay curves fitted by the sum of two exponential components have different decay times.

$$I = A_1 \exp(-t/\tau_1) + A_2 \exp(-t/\tau_2) \quad (4)$$

where, I is phosphorescence intensity, A_1, A_2 are constants, t is time, τ_1 and τ_2 are decay times (in second) for the exponential components [30]. Afterglow curves are successfully fitted by the equation (4) and the fitting curve result are shown in Table 3. Using the fitting function provided by ORIGIN8 software, t he calculated afterglow decay for the mentioned compound s was found. The results indicated that the prepared $Sr_2SiO_4:Dy^{3+}_{(2.0\%)}$ phosphor shows a rapid decay and the long lasting phosphorescence.

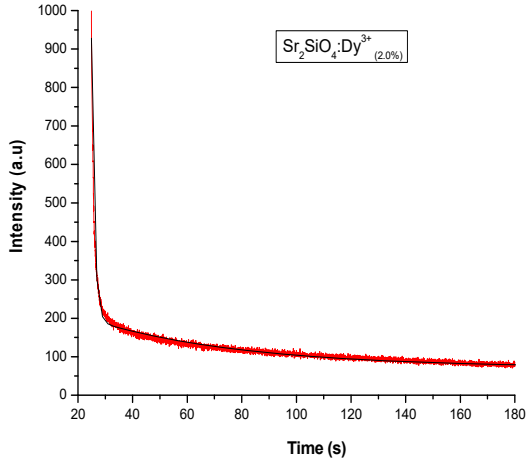

Fig. 9 Afterglow curves of $SrSiO_3:Dy^{3+}$ phosphor

Table 3 Fitting results of the afterglow curves

Phosphor	τ_1 (s)	τ_2 (s)
$Sr_2SiO_4:Dy^{3+}_{(2.0\%)}$	1.07	55.95

Dy^{3+} is an important rare earth ion in the development of phosphors with long lasting afterglow, playing a crucial role. It is reasonable to consider that the role of doping Dy^{3+} ions is to introduce new types of traps or significantly increase the concentration of traps responsible for the afterglow [31]. The afterglow intensity of the persistent phosphor depends on the densities of the traps electrons, while the duration of afterglow depends on the depth of the trapped electrons. For a suitable trap depth, the trap concentration is directly depends on the dysprosium ions [32].

Mechanoluminescence (ML)

ML also known as Triboluminescence, has been observed in many kinds of solids including ionic crystals, semiconductors, metals, glasses and organic crystals [33]. In the present studies, an impulsive deformation technique has been used. During the deformation of a solid, a great number of physical processes may occur within very short time intervals, which may excite or stimulate the process of photon emission [34]. When a moving piston is applied to the phosphor, initially the ML intensity increases with time, attains a peak value and then decreases with time. Such a curve between the ML intensity and deformation time of phosphors is known as the ML glow curve [35].

Fig. 10 (a) shows that the characteristic curve between ML intensity versus time for different heights (h = 10, 20, 30, 40, 50 cm). The phosphor was fractured via dropping a load [moving piston] of particular mass (400 g) and cylindrical shape on the $Sr_2SiO_4:Dy^{3+}_{(2.0\%)}$ phosphor. The velocity of the moving piston, holding the impact mass, could be changed, by changing the height through which it was dropped. Every time for the ML measurement, the quantity of $Sr_2SiO_4:Dy^{3+}_{(2.0\%)}$ phosphor was kept constant (8 mg). When the moving piston is dropped onto the prepared phosphor at different height, light is emitted. The photon emission time is nearly 2 ms, when prepared $Sr_2SiO_4:Dy^{3+}$(2.0%) phosphor fractures. Maximum ML intensity has been obtained for the 50 cm dropping height and ML intensity increases linearly with the increases the falling height of the moving piston. The sintered $Sr_2SiO_4:Dy^{3+}$ (2.0%) phosphor was not irradiated by any excitation source [36].

Fig. 10 (b) shows the characteristics curve of ML intensity versus impact velocities for the phosphor. ML intensity increases linearly with increasing impact velocity [$\sqrt{2gh}$, (where "**g**" is the acceleration due to gravity and "**h**" is the height through which the load is dropped freely)] of the moving piston. The ML intensity of $Sr_2SiO_4:Dy^{3+}_{(2.0\%)}$ phosphor increases linearly with increasing the mechanical stress [37].

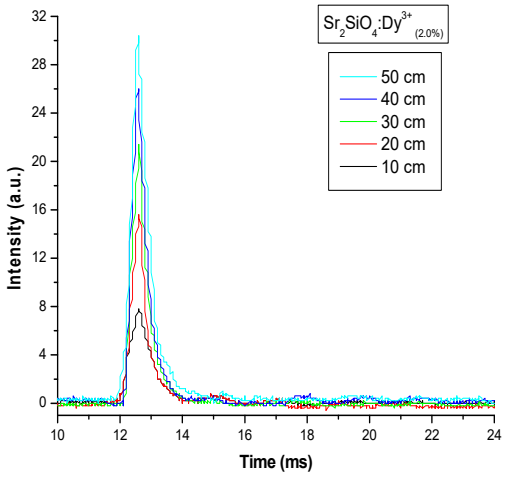

Fig. 10(a) ML intensity versus time curve of $Sr_2SiO_4:Dy^{3+}_{(2.0\%)}$ phosphor

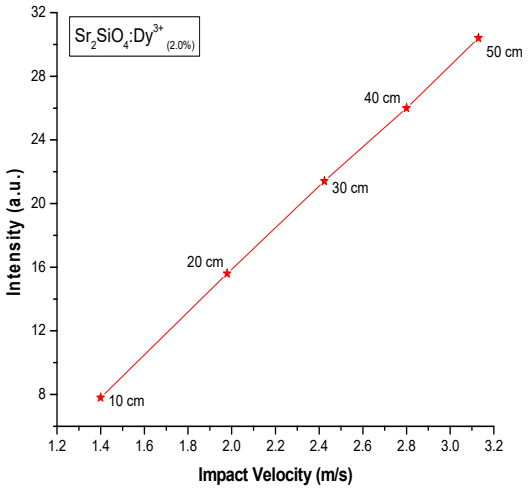

Fig. 10 (b) ML intensity versus impact velocity curve of $Sr_2SiO_4:Dy^{3+}_{(2.0\%)}$ phosphor

When the load or piston makes an impact on the crystal with an initial velocity v_0, the former decelerates and after a particular time its velocity becomes zero. The time dependence of the velocity of the piston may be written as

$$v = v_0 \exp(-\beta v_o t) \quad (5)$$

Where β is a constant, equation (4) can be written as

$$\frac{dx}{dt} = v_0 \exp(-\beta v_o t) \quad (6)$$

Where dx is the compression of the crystal during the time interval dt.

Integrating equation (5), we have

$$x = \frac{1}{\beta}\exp(-\beta v_o t) + C \quad (7)$$

x = 0 for t = 0, therefore, equation (6) may be written as

$$x = \frac{1}{\beta}[1 - \exp(-\beta v_o t)] \quad (8)$$

The prepared phosphor is in powder form and the impact velocities compress it to a certain extent, but this does not change significantly with increasing impact velocity. Equation (7) shows that impact time remains mostly unchanged with increasing impact velocity because there is no significant change in compression, which is expressed by 'x' in equation (8). This may be one reason why, the time that corresponds to the peak ML intensity, does not change significantly with increasing impact velocity.

Fig. 11 shows the time corresponding to ML signal peak with impact velocity of $Sr_2SiO_4:Dy^{3+}_{(2.0\%)}$ phosphor. It can be seen that time for peak ML intensity does not change significantly with increasing impact velocity [38].

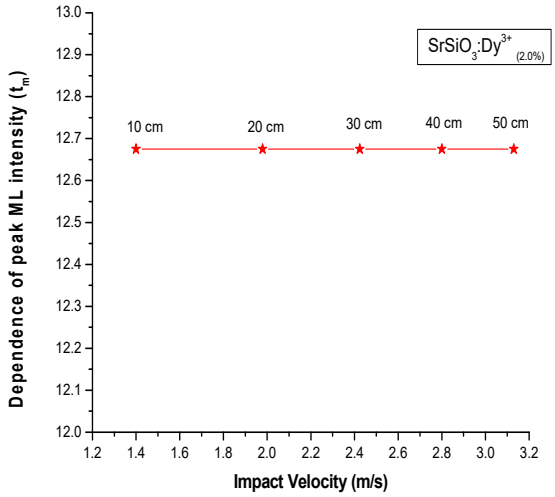

Fig. 11 Variiton of Time corresponds to ML signal peak with impact velocity of $Sr_2MgSi_2O_7:Eu^{3+}$ phosphor

The relationship between semi-log plot of ML intensity versus $(t–t_m)$ for $Sr_2SiO_4:Dy^{3+}_{(2.0\%)}$ phosphor is shown in Fig. 12, and the lines were fitted using the following equation,

$$\tau = \frac{1}{slop \quad of \quad straight \quad line} \quad (8)$$

Curve fitting results show that decay constant (τ) varies from 0.80 to 0.84 ms. (Table 4).

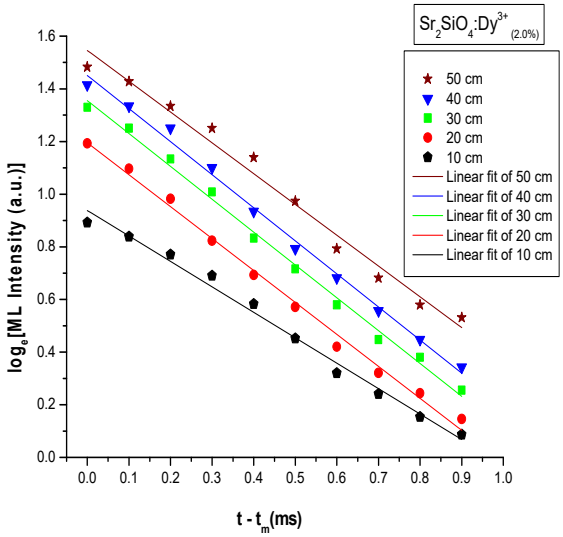

Fig. 12 Semi-log plot of ML intensity versus $(t – t_m)$ for $Sr_2SiO_4:Dy^{3+}_{(2.0\%)}$ phosphor

Table 4 Calculation of ML decay constant

Impact velocity	10 cm	20 cm	30 cm	40 cm	50 cm
τ Decay constant(ms)	1.11	0.83	0.83	0.83	0.91

When a mechanical stress, such as compress, friction, and striking, and so on, was applied on the sintered $Sr_2SiO_4:Dy^{3+}_{(2.0\%)}$ phosphors, piezo-electric field can be produced. Therefore, in such phosphor the ML excitation may be caused by the local piezoelectric field near the impurities and defects in the crystals. During the impact on the material, one of its newly created surfaces gets positively charged and the other surface of the crack gets negatively charged. Thus, an intense electric field of the order of 10^6 - 10^7 Volt cm^{-1} is produced [see Fig.13].

Under such order of electric field, the ejected electrons from the negatively charged surface may be accelerated and subsequently their impact on the positively charged surfaces may excite the luminescence center such as Eu^{3+} [39]. Subsequently, the de-excitation of excited Eu^{3+} ions may give rise to the light emission due to the transition from excited state to ground state.

With the increasing impact velocity, more compression of the sample takes place, and therefore, more area of the newly created surface takes place. Thus, the ML intensity will increase with increasing value of the impact velocity. It is to be noted that the stress near the tip of a moving crack is of the order of $Y/100 \approx 10^{10}$ dynes/cm^2 = 10^9 Newton/m^2 (where Y is the Young's modulus of the materials). Thus a fixed charge density will be produced on the newly created surfaces and the increase in the ML intensity will primarily be caused by the increase in the rate of newly created surface area with increasing impact velocity. Moreover, the total ML intensity will also increase with impact velocity because more compression of the sample will create more surfaces with increasing impact velocity [40].

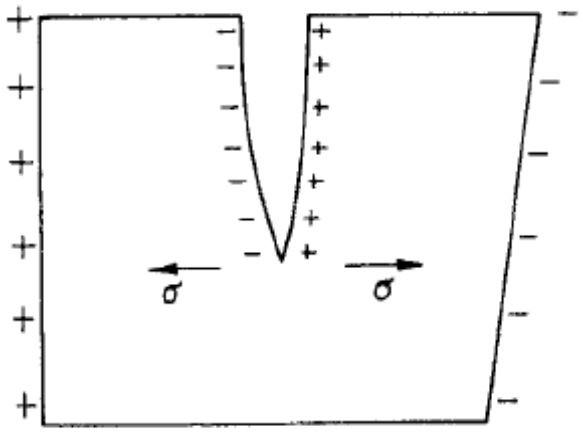

Fig. 13 Langevin model for the piezo-electrification induce phosphor

As the impact velocity increases, the impact pressure also increases leading to the increase in the electric field at local region which causes the decrease in trap depth. Hence the probability of de-trapping increases. From Fig. 10, it can be seen that with increasing impact velocity, ML intensity also increases linearly i.e., the ML intensity of $Sr_2SiO_4:Dy^{3+}$ (2.0%) phosphor are linearly proportional to the magnitude of the impact velocity, which suggests that this phosphor can be used as sensor to detect the stress of an object.

CONCLUSION

In summary, $Sr_2SiO_4:xDy^{3+}$ phosphor was prepared by the high temperature solid state reaction method. The monoclinic structure of the phosphor was confirmed by the XRD. The surface of the phosphor showed irregular shapes. EDS spectrum confirmed the elements present in synthesized $Sr_2SiO_4:Dy^{3+}$ phosphor. Under the ultra-violet (UV) excitation, the phosphor would emit blue, yellow and red light with peak at 480 nm and 576 nm corresponds to the transitions of $^4F_{9/2} \rightarrow {}^6H_{15/2}$ and $^4F_{9/2} \rightarrow {}^6H_{13/2}$ respectively. The calculated CIE coordinates were found to be very close to standard white light. $Sr_2SiO_4:Dy^{3+}$ (2.0%) phosphor, as calculated by a curve fitting technique, has different decay times (τ_1 = 1.07 s; τ_2 = 55.59 s) with fast and slow decay processes. The dependence between ML intensity of $Sr_2SiO_4:Dy^{3+}$ (2.0%) phosphor to the impact velocity is close to linearity, which suggests the probable use of this phosphor as sensor to detect the stress of an object.

References:

1. P. You, G. Yin, X. Chen, B. Yue, Z. Huang, X. Liao, Y. Yao, Optical Materials 2011; 33: 1808–1812.
2. M. A. Tshabalala, F. B. Dejene, S. S. Pitale, H.C.Swart, O. M. Ntwaeaborwa, Physica B 2014; 439: 126–129.

3. G. Zhu,Y. Wang, Q. Wang, X. Ding, W. Geng, Y. Shi, Journal ofLuminescence, 2014; 154: 246–250.
4. V. B. Pawade, S. J. Dhoble, Journal of Luminescence 2014; 145: 626–630.
5. Y. Liu, B. Lei, C. Shi, Chem. Mater. 2005; 17: 2108-2113.
6. B. Liu, L. Kong, C. Shi, Journal of Luminescence, 2007;122–123: 121–124.
7. C. N. Xu, T. Wantanabe, M. Akiyama, and X. G. Zheng, Appl. Phys. Lett. 1999; 74: 1236 – 1238.
8. I. P. Sahu, D. P. Bisen, N. Brhame, R.K. Tamrakar, R. Shrivastava J Mater Sci: Mater Electron, (2015), DOI 10.1007/s10854-015-3563-5.
9. C. N. Xu, T. Wantanabe, M. Akiyama, and X. G. Zheng, Appl. Phys. Lett. 1999; 74: 2414-2416.
10. C. N. Xu, X. G. Zheng, M. Akiyama, K. Nonaka, and T. Wantanabe, Appl. Phys. Lett. 2000; 76: 179 – 181
11. C. N. Xu, X. G. Zheng, T. Wantanabe, M. Akiyama, I. Usui, Thin Solid Films 1999; 352: 273 -278.
12. I P. Sahu, D. P. Bisen, N. Brahme, M. Ganjir, Lumin. J. Biol. Chem. Lumin. 2015; DOI 10.1002/bio.2900
13. S.W.S. McKeever, Radiation Measurements, 2011; 46: 1336-1341.
14. I. P. Sahu,
15. JCPDS file number 75 - 1736, JCPDS International Center for Diffraction Data.
16. S. Basuna, G.F. Imbuschb, D.D. Jiac, W.M. Yenc, J. Lumin. 104 (2003) 283.
17. R. Chen, Y. Kirsh, Pergamon Press (1981) 167.
18. R. Chen, S.W.S. McKeever, World Scientific (1997).
19. A. Mandowski, A.J.J. Bos, Radiation Measurements 2011; 46: 1376-1379.
20. C. Y. Li, Q. Su, J. R. Qiu, J. Lumin. 24 (2003) 19.
21. H. N. Luitel, T. Watari, R. Chand, T. Torikai, M. Yada, J. Mater. 2013 (2013) 10.
22. I. P. Sahu, D. P. Bisen, N. Brahme, Displays, 2014; 35: 279 – 286.
23. A. K. Parchur, R.S. Ningthoujam, Dalton Trans. 40 (2011) 7590.
24. N. N. Yamashita, J. Phys. Soc. Jpn. 1973; 35: 1089.
25. J. Kuang, Y. Liu, J. Zhang, Journal of Solid State Chemistry 2006; 179: 266–269
26. G. S. Rama Raju, J. Y. Park, H. C. Jung, B. K. Moon, J. H. Jeong, J. H. Kim, Curr. Appl Phys. 2009; 9: 92.
27. Y. Chen, X. Cheng, M. Liu, Z. Qi, C. Shi, Journal of Luminescence 2009; 129: 531–535.
28. A. Zukauskas, M.S. Shur, R Gaska. Introduction to Solid State Lighting, Wiley: New York, 2002..
29. CIE, International Commission on Illumination, Publication CIE no. 15, (E-1.3.1), 1931
30. R. Shrivastava, J. Kaur, M. Dash, Superlattices and Microstructures 2015; 82: 262–268.
31. A. H. Wako, B. F. Dejene, H. C. Swart, Physica B 2014; 439: 153–159.
32. Y. Lin, Z. Zhang, Z. Tang, J. Zhang, Z. Zheng, X. Lu, Materials Chemistry and Physics 2001;70: 156–159.
33. Yi Jia, M. Yei, W. Jia, Optical Materials 2006; 25: 974–979.
34. D.R. Vij, Luminescence of Solids, Plenum Press, New York (1998).
35. V.K. Chandra, B.P. Chandra, Optical Materials, 2011; 34: 194–200
36. I. P. Sahu, D. P. Bisen, N. Brahme, Lumin. J. Biol. Chem. Lumin. 2015; 30 (5): 526-532.
37. Zhang H, Yamada H, Terasaki N, Xu C N, Int. J. Mod Phys B, 2009; 23 (6-7): 1028 – 1033.
38. R. Shrivastava, J. Kaur, B. P. Chandra, Lumin. J. Biol. Chem. Lumin. 2015; DOI 10.1002/bio.2882.
39. H. Zhang, H. Yamada, N. Terasaki, C.N. Xu, Thin Solid Films 518 610 – 613 (2009).
40. I. P. Sahu, D. P. Bisen, N. Brahme, R. K. Tamrakar, J. Lumin, 2015; 167: 278-288.